ACS Sustainable Chemistry & Engineering

Research Article

pubs.acs.org/journal/ascecg

A Novel Flexible Supercapacitor Based on Cross-Linked PVDF-HFP Porous Organogel Electrolyte and Carbon Nanotube Paper@π-Conjugated Polymer Film Electrodes

Chongyang Yang, Minqiang Sun, Xi Wang, and Gengchao Wang*

Key Laboratory for Ultrafine Materials of Ministry of Education, Shanghai Key Laboratory of Advanced Polymeric Materials, School of Materials Science and Engineering, East China University of Science and Technology, Shanghai 200237, P.R.China

Supporting Information

ABSTRACT: High energy density and safety are the goals in the pursuit of flexible energy storage devices. Herein, we report a novel flexible supercapacitor (SC) fabricated with a cross-linked poly(vinylidene fluoride-*co*-hexafluoropropylene) (PVDF-HFP) porous organogel electrolyte and carbon nanotube paper@poly(1,5-diaminoanthraquinone) (CNT@PDAA) film electrodes. The PVDF-HFP/tetraethylammonium tetrafluoroborate-acetonitrile (Et_4NBF_4-AN) organogel electrolyte, featured with a highly porous structure and chemical cross-linking, exhibits nonflammability, a broad electrochemical stable window, and high ionic conductivity of 14.4×10^{-3} S cm^{-1}, as well as improved solvent resistance. The CNT@PDAA electrode displays good pseudocapacitive performance in a broad potential window due to p- and n-doping characteristics. Because of this rational design, the as-prepared flexible SC device achieves an excellent volumetric capacitance of 5.2 F cm^{-3} and a high energy density of 5.16 mWh cm^{-3} (41.4 Wh kg^{-1}) at a power density of 0.051 W cm^{-3} (0.41 kW kg^{-1}). More importantly, a unit of as-assembled SC is shown to drive a commercially available product even in a bent state.

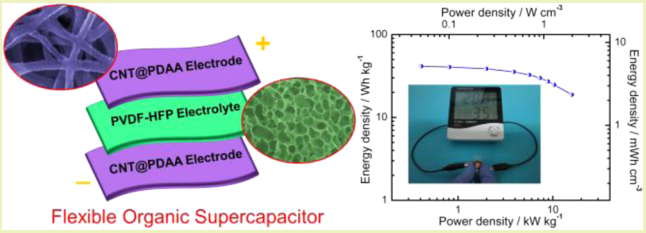

KEYWORDS: *Poly(vinylidene fluoride-co-hexafluoropropylene), Organogel electrolyte, Cross-linked, Irradiation, Poly(1,5-diaminoanthraquinone), Flexible supercapacitor*

INTRODUCTION

Owing to large proliferation of wearable and stretchable electronic products, typically collapsible displays, electronic paper, and wearable systems for personal multimedia, the demand for versatile flexible energy storage devices has arisen.[1−4] Supercapacitors (SCs) using the gel polymer electrolyte (GPE) are promising due to the merits of being lightweight, flexible, and portable.[5−8] Although the power density of SCs is much higher than that of lithium-ion batteries (LIBs), their energy density is far from satisfactory.[9,10] Nowadays, much research on SCs aims at fabricating flexible SCs as well as increasing energy density.[11−14]

According to the equation of $E = 1/2CU^2$, obviously, the energy density can be improved by maximizing the device capacitance (C) and/or the potential window (U).[15,16] An efficient approach is to use GPEs containing organic electrolytes for flexible SCs.[17,18] Various polymers including poly(ethylene oxide) (PEO),[19] poly(methyl methacrylate) (PMMA),[20] poly(acrylonitrile) (PAN),[21] poly(vinyl chloride) (PVC),[22] poly(vinylpyrrolidone) (PVP),[23] poly(vinylidene fluoride) (PVDF),[24−26] and poly(vinylidene fluoride-*co*-hexafluoropropylene) (PVDF-HFP)[26−28] have been investigated as GPE matrices. Among these, PVDF-HFP, with crystalline parts (PVDF) to maintain the mechanical property and amorphous parts (PHFP) to trap the liquid electrolyte, is widely used because of its nonflammability, good electrochemical stability, and affinity to polar liquid electrolytes.[29−31]

The porous PVDF-HFP gel electrolyte, prepared through impregnating the porous PVDF-HFP membrane matrix with the electrolyte solution, has been regarded as one of the promising organogel electrolytes.[31−35] Unfortunately, the PVDF-HFP membranes mostly present poor mechanical properties because they are easily softened after uptake of liquid electrolytes such as acetonitrile (AN),[36] leading to internal short circuits. Thus, cross-linked PVDF-HFP membranes are expected to be more dimensionally stable. However, to our knowledge, there are no reports on the porous PVDF-HFP electrolyte cross-linked by irradiation method for flexible SCs.

On the other hand, carbonaceous materials are usually employed as electrode materials for flexible SCs with organic electrolytes due to their wide potential window.[37−39] Unfortunately, the low specific capacitance gives rise to unsatisfactory energy density. Coupling conducting polymers (CPs) to flexible carbonaceous electrodes can significantly improve the specific capacitance of flexible SCs.[40−43] However,

Received: April 20, 2015
Revised: July 9, 2015
Published: July 17, 2015

DOI: 10.1021/acssuschemeng.5b00334
ACS Sustainable Chem. Eng. 2015, 3, 2067−2076

CPs with a p-doping characteristic, such as polyaniline (PANI) and polypyrrole (PPy), only exhibit high pseudocapacitance in a narrow potential window.[44] Recently, poly(1,5-diaminoanthraquinone) (PDAA), containing a moiety of 1,4-benzoquinone (n-type doping) and two moieties of aniline (p-type doping), possesses an excellent pseudocapacitance characteristic over a broader potential range compared with PANI and PPy.[44−50] Moreover, due to strong hydrogen bonds and a $\pi-\pi$ stacking interaction among anthracene rings and hydrogen bonds, PDAA tends to form a supramolecular structure, leading to outstanding cycling stability compared to other reported CPs.[44,45,50]

Herein, we ingeniously designed a novel organic flexible supercapacitor (SC) based on a cross-linked poly(vinylidene fluoride-*co*-hexafluoropropylene) (PVDF-HFP) porous organogel electrolyte and carbon nanotube paper@poly(1,5-diaminoanthraquinone) (CNT@PDAA) film electrodes. The cross-linked PVDF-HFP porous membrane was prepared via a dual-coagulation bath by the phase inversion technique, followed by radiation cross-linking with trimethylolpropane triacrylate (TMPTA) as the cross-linking agent. The CNT@PDAA film electrodes were facilely synthesized by the electrochemical polymerization strategy and served as both positive and negative electrodes for organic flexible SC. The as-fabricated SC delivers a high energy density of 41.4 Wh kg^{-1} at a power density of 0.41 kW kg^{-1} and functions well both in the flat and bent state.

EXPERIMENTAL SECTION

Preparation of Cross-Linked PVDF-HFP Porous Membrane. The PVDF-HFP porous membranes were prepared by immersion precipitation. First, the PVDF-HFP (Kynar Powerflex LBG, Elf Atochem, M_w = 450,000 g mol^{-1}, 1.78 g cm^{-3}) and polyvinylpyrrolidone (PVP) were dissolved in dimethylacetamide (DMAc). The concentrations of PVDF-HFP and PVP were 16 and 4 wt %, respectively. The solution was cast onto a glass plate with a doctor knife. The plate was first immersed in a water/alcohol (V/V = 1/1) bath for 10 min and passed through a water bath to complete the solidification process. Then, the obtained porous membrane was immersed in ethanol and hexane, followed by air drying at ambient temperature. After immersion in a butanol solution of 2.5 wt % trimethylolpropane triacrylate (TMPTA), the PVDF-HFP porous membrane was cross-linked by ^{60}Co γ-ray irradiation with a dose of 100 kGy under argon atmosphere. Successively, the homopolymer of the cross-linker in the PVDF-HFP porous membrane was removed by extraction with chloroform in a Soxhlet apparatus. Finally, the membrane was immersed in hexane, followed by drying in vacuum.

Preparation of CNT@PDAA Flexible Film Electrodes. CNT@PDAA film electrodes were prepared by the electropolymerization method. Prior to electropolymerization, CNT films (diameter of CNT = 15−30 nm, Suzhou Creative Nano Carbon of China) were cleaned with ethanol. Then, the CNT paper of 1 cm × 1 cm, Pt sheet of 2 cm × 2 cm, and Ag/Ag^+ electrode (containing 0.01 M $AgNO_3$ of acetonitrile, +0.300 V versus a saturated calomel electrode) were used as the working, counter, and reference electrodes, respectively. Poly(1,5-diaminoanthraquinone) (PDAA) was potentiostatically electropolymerized at +1.2 V (vs Ag/Ag^+) on CNT paper in an acetonitrile (AN) solution containing 5 mM 1,5-diaminoanthraquinone (DAA) monomer, 0.1 M tetraethylammonium tetrafluoroborate (Et_4NBF_4), and 0.5 M trifluoroacetic acid (CF_3COOH) for different charge densities (0.7, 1.0, 1.5, 2.0, 2.5, and 3.0 C cm^{-2}). The electropolymerization was performed in an argon-filled glovebox. For comparison, pure PDAA was directly electropolymerized on a Pt sheet through a similar procedure as above.

Assembly of Flexible Supercapacitors. Prior to assembling flexible SCs, the cross-linked PVDF-HFP porous membrane and CNT@PDAA film electrodes were immersed in 1 M tetraethylammonium tetrafluoroborate-acetonitrile (Et_4NBF_4-AN). The CNT@PDAA film electrodes were first laminated onto both sides of a PVDF-HFP electrolyte, and then two copper foils were covered closely on the film electrodes to function as current collectors, sealed by a polydimethylsiloxane (PDMS) membrane. Here, the PDMS membrane was fabricated by vigorously mixing a silicone-elastomer base and curing agent (Sylgard 184, Dow Corning) at a weight ratio of 10:1, followed by degassing in a vacuum oven for 30 min and thermally curing at 80 °C for 5 h. The assembly was carried out in an argon-filled glovebox. The CNT@PDAA film with a constant charge density of 2.5 C cm^{-2} was chosen as the positive electrode. The CNT@PDAA films grown for 0.7, 1, 1.5, 2, and 2.5 C cm^{-2} were used as negative electrodes, respectively, which were labeled as SC-0.7, SC-1.0, SC-1.5, SC-2.0, and SC-2.5 for flexible SCs. If not specified, the flexible SC in this paper stands for SC-1.5. To compare the electrochemical performance of the PVDF-HFP organogel electrolyte and liquid-phase electrolyte with polypropylene separator (Celgard 3501, 25 μm), symmetric SCs based on CNT electrodes were fabricated.

Characterization. The morphologies of the samples were observed by field-emission scanning electron microscopy (FE-SEM, Hitachi S4800). The Fourier transform infrared spectroscopy (FTIR) spectra were characterized using a Nicolet 6700 spectrometer equipped with a Smart OMNI Sampler. X-ray diffraction (XRD) data were collected from 3° to 50° (2θ) by a Rigaku D/Max 2550 VB/PC X-ray diffractometer using Cu Kα radiation. Differential scanning calorimetry (DSC) analysis was performed on a Modulated DSC2910 at a heating rate of 10 °C min^{-1} under nitrogen atmosphere. The weight loss of the samples were measured using a thermogravimetric analyzer (TGA, NET-ZSCH STA 449 C) from room temperature to 800 °C at a heating rate of 10 °C min^{-1} under nitrogen atmosphere. The mechanical properties of the PVDF-HFP membranes were carried out on a Zwick Roell testing system at a tensile speed of 5 mm min^{-1}.

The ionic conductivity of the PVDF-HFP gel electrolytes was obtained by the blocking stainless steel (SS)//PVDF-HFP/Et_4NBF_4-AN//SS model device using electrochemical impedance spectroscopy (EIS) with an AC amplitude of 5 mV from 10^5 to 1 Hz. The ionic conductivity (σ) was calculated from the bulk resistance (R_b, Ω) according to following equation:

$$\sigma = L/(R_b \times S) \tag{1}$$

where L is the thickness (cm) of the organogel, S is the effective contact area (cm^2), and R_b is obtained from the Nyquist plot.

The Et_4NBF_4-AN electrolyte uptake was calculated according to following equation:

$$\text{electrolyte uptake} = (W_w - W_d)/W_d \times 100\% \tag{2}$$

where W_d is the dry weight of PVDF-HFP porous membrane dried in a vacuum oven at 60 °C, and W_w is the wet weight of PVDF-HFP membrane immersed in Et_4NBF_4-AN.

The swelling ratio of the membrane was calculated according to following equation:

$$\text{swelling ratio} = (D_w - D_d)/D_d \times 100\% \tag{3}$$

where D_d and D_w are the diagonal length of dry and swollen membranes, respectively.

Porosity of the porous membranes was tested by the *n*-butanol adsorption method. The weighed membranes were immersed in *n*-butanol for 2 h. Then, the membrane surface was dried by filter paper and weighed again. Porosity was calculated according to following equation:

$$\text{porosity}\ (\%) = \frac{(m_w - m_d)/\rho_n}{(m_w - m_d)/\rho_n + m_d/\rho_p} \times 100\% \tag{4}$$

where m_w and m_d are the weights of the wet and dry membranes, respectively, and ρ_n and ρ_p are the densities of *n*-butanol and PVDF-HFP, respectively.

DOI: 10.1021/acssuschemeng.5b00334
ACS Sustainable Chem. Eng. 2015, 3, 2067−2076

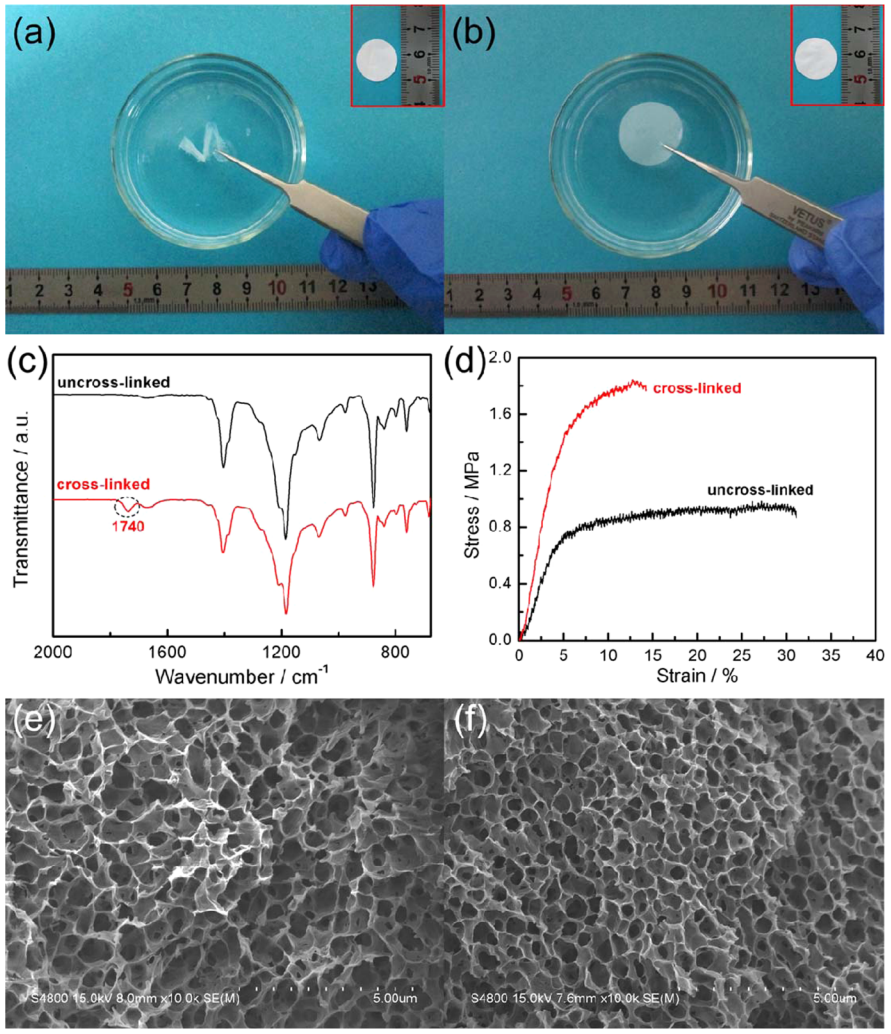

Figure 1. Digital photos of (a) PVDF-HFP and (b) cross-linked PVDF-HFP porous membranes after being immersed in acetonitrile at 50 °C (inserted photos show the membranes before immersion). (c) FTIR spectra and (d) stress−strain curves of PVDF-HFP and cross-linked PVDF-HFP porous membranes. FESEM images of (e) PVDF-HFP and (f) cross-linked PVDF-HFP porous membranes.

Electrochemical Measurements. Cyclic voltammetry (CV), galvanostatic charge−discharge, and electrochemical impedance spectroscopy (EIS) measurements were achieved on a CHI 660D electrochemical workstation in a two-electrode mode. Cycling stability of the flexible SCs was performed on a LAND CT2001A program testing system. It is worth noting that the specific capacitance, energy, and power density were calculated based on the total mass of positive and negative electrodes. In a three-electrode system, a Pt sheet and Ag/Ag^+ electrode were used as the counter and reference electrodes, respectively. The cyclic voltammetry and galvanostatic charge−discharge tests were performed inside an argon-filled glovebox. Data analyses for electrochemical measurements are shown in the Supporting Information.

RESULTS AND DISCUSSION

The influence of ^{60}Co γ-ray irradiation on the cross-linking, morphology, structure, and mechanical property of porous membranes was investigated. As shown in Figure 1a, the nonirradiated PVDF-HFP membrane is severely damaged after being immersed in an acetonitrile solution for 1 h. In contrast, the irradiated PVDF-HFP membrane is intact and exhibits slight swelling with a swelling ratio of 11% after immersion for 24 h (Figure 1b). The above results confirm that the PVDF-HFP was successfully cross-linked after irradiation. The chemical structures of PVDF-HFP and irradiated PVDF-HFP membranes were studied by means of ATR-FTIR spectra. For the nonirradiated PVDF-HFP membrane, the characteristic absorption peaks at 1184 and 1411 cm^{-1} corresponding to the C−F stretching vibrations were observed (Figure 1c).[51] However, the irradiated membrane gives an extra peak at about 1740 cm^{-1}, which is assigned to the stretching vibration of carbonyl groups, indicating the existence of TMPTA in the PVDF-HFP matrix. The FTIR analysis further proves the cross-linking of the PVDF-HFP membrane by TMPTA after irradiation.

To emphasize the effect of cross-linking on mechanical performance of the PVDF-HFP membrane, a tensile test was carried out (Figure 1d). The tensile strength (1.80 MPa) of the cross-linked PVDF-HFP membrane is twice that of the nonirradiated membrane (0.94 MPa), indicating the improved tensile strength through cross-linking. However, cross-linking causes a decrease in elongation-at-break of the PVDF-HFP membrane. As shown in Figure S1, little variation of the XRD peaks for PVDF-HFP membranes was observed before and after cross-linking. DSC analysis exhibits that both uncross-linked and cross-linked membranes display a similar melting behavior around 150 °C, and the melting enthalpy of the cross-

DOI: 10.1021/acssuschemeng.5b00334
ACS Sustainable Chem. Eng. 2015, 3, 2067−2076

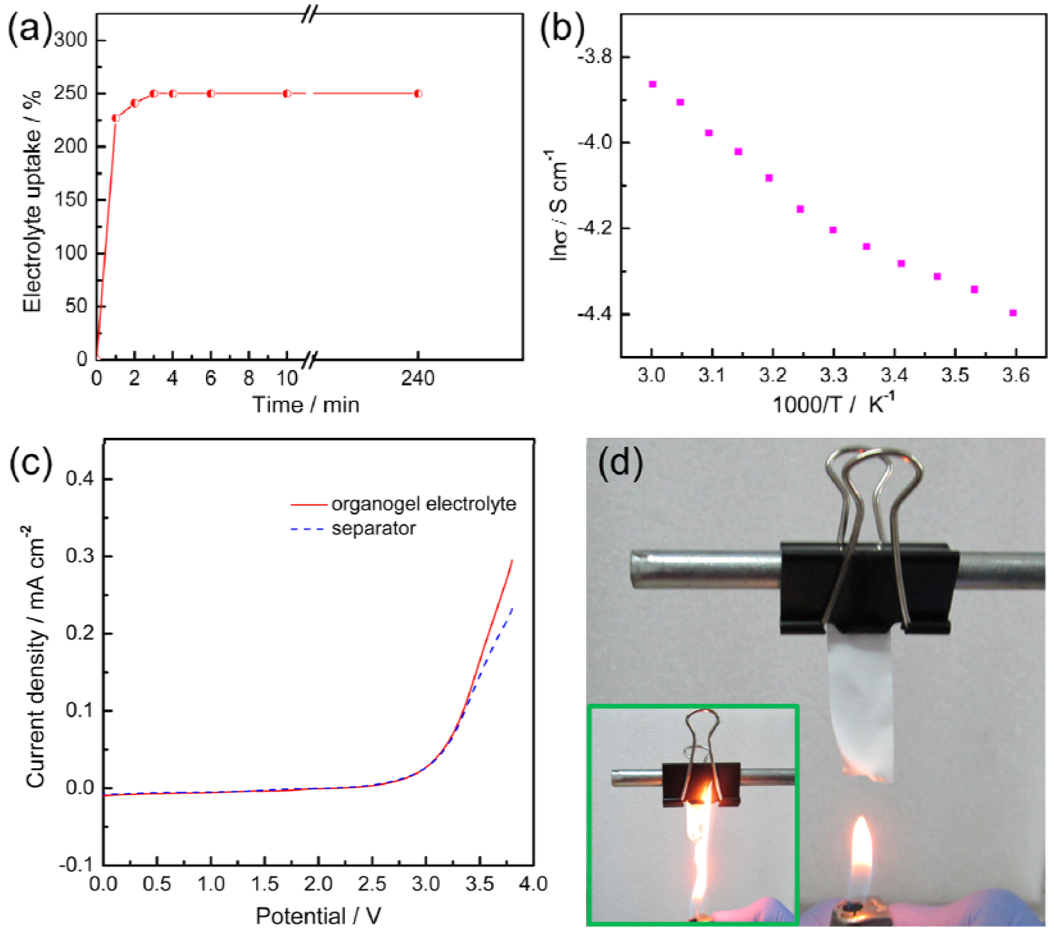

Figure 2. Characterization of the cross-linked PVDF-HFP/Et_4NBF_4-AN electrolyte. (a) Electrolyte uptakes at various immersing times for the cross-linked PVDF-HFP porous membrane. (b) Temperature dependence of conductivity. (c) Linear sweep voltammograms of the PVDF-HFP/Et_4NBF_4-AN electrolyte and separator with the Et_4NBF_4-AN electrolyte using stainless steel as working electrodes at 5 mV s^{-1}. (d) Flammability test of the PVDF-HFP/Et_4NBF_4-AN electrolyte. Inset shows the flammability test of the separator with the Et_4NBF_4-AN electrolyte.

linked membrane decreases slightly (Figure S2). These results indicate that cross-linking has a small effect on crystallization behavior.

To shed light on the influence of irradiation on the morphologies of PVDF-HFP membranes, FE-SEM analysis was employed. As shown in Figure 1e, the uncross-linked PVDF-HFP membrane presents a highly and uniformly interconnected porous structure with a pore size from 0.8 to 1 μm. Interestingly, the cross-linked PVDF-HFP membrane exhibits a very similar porous structure with a porosity of ca. 75%. However, the pore diameter of the cross-linked membrane slightly reduces to about 600 nm (Figure 1f). The submicron porous and interconnected skeleton structure of the membranes functions as an interconnected framework to transport ions and provides the ability to absorb abundant electrolytes.

The PVDF-HFP organogel electrolyte was obtained by impregnating the cross-linked PVDF-HFP porous membrane in 1 M Et_4NBF_4-AN electrolyte, and the performance of the PVDF-HFP organogel electrolyte was evaluated, as shown in Figure 2. Surprisingly, the cross-linked PVDF-HFP porous membrane absorbs the liquid electrolyte rapidly and reaches maximum electrolyte uptake of 250 wt % in a few minutes (Figure 2a). This is attributed to the perfectly interconnected porous structure of the cross-linked PVDF-HFP membrane. Figure 2b illustrates the temperature dependence of the ionic conductivity of the PVDF-HFP organogel electrolyte. The ionic conductivity increases with temperature in accord with the Arrhenius relationship. The ionic conductivity of the PVDF-HFP electrolyte reaches up to 14.4×10^{-3} S cm^{-1} at 25 °C, which is high enough to be applied in an organic flexible SC. The high ionic conductivity of the PVDF-HFP organogel electrolyte can be explained as follows: (1) The liquid Et_4NBF_4-AN electrolyte with high ionic conductivity (~55×10^{-3} S cm^{-1})[52] was absorbed in the organogel electrolyte. (2) The absorbed liquid electrolyte in the porous membrane exists in a free liquid state within the pores of the membrane and in the swollen PVDF-HFP gel space. The high porosity and cross-linked structure of the PVDF-HFP membrane lead to high electrolyte uptake. (3) The open and interconnected porous structure of the PVDF-HFP membrane with submicron pore size facilitated ion motion in the gel electrolyte.[53,54]

The stable potential window of the electrolyte is vital to improve the energy density of the supercapacitor. Figure 2c depicts the linear sweep voltammetry curves of the cross-linked PVDF-HFP/Et_4NBF_4-AN and separator with liquid Et_4NBF_4-AN electrolytes sandwiched between stainless steel electrodes. It is found that both PVDF-HFP/Et_4NBF_4-AN and Et_4NBF_4-AN electrolytes are stable at the potential between 0 and 2.9 V, which is acceptable for supercapacitors using AN electrolyte.[55] The flame resistance is essential for the supercapacitor and especially for the organic supercapacitor at a thermal incident.

DOI: 10.1021/acssuschemeng.5b00334
ACS Sustainable Chem. Eng. 2015, 3, 2067−2076

For this purpose, the flammability of the cross-linked PVDF-HFP organogel electrolyte was tested. As shown in Figure 2d, the PVDF-HFP organogel electrolyte presents a remarkable resistance to the flame. This excellent flame-retarding ability is attributed to the self-extinguishing property of the PVDF-HFP membrane. In contrast, the polypropylene separator impregnated with the Et_4NBF_4-AN electrolyte ignited instantaneously and was completely engulfed in flame.

To investigate the electrochemical performance of the PVDF-HFP organogel electrolyte, symmetric electrical double layer capacitors based on CNT electrodes were fabricated. Figure 3a shows that a SC with an organogel electrolyte has

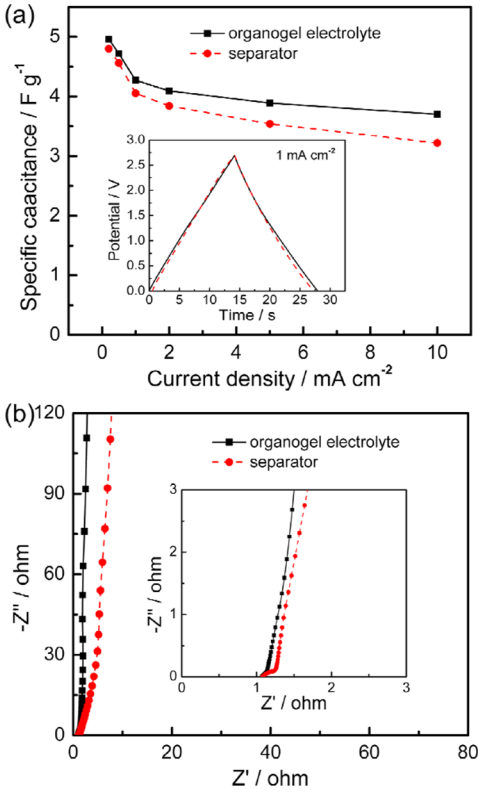

Figure 3. (a) Specific capacitances and (b) Nyquist plots of CNT//PVDF-HFP/Et_4NBF_4-AN//CNT and CNT//Separator/Et_4NBF_4-AN//CNT SCs. Inset in (a) shows galvanostatic charge−discharge curves of the SCs at 1 mA cm^{-2}. Inset in (b) shows a magnified view of the high frequency region of the impedance spectra.

better capacitance retention than that with a liquid electrolyte as the current density increases. The specific capacitances of the two SCs are similar (4.25 and 4.05 F g^{-1}). The charge curves of both SCs were almost symmetrical with their corresponding discharge curves within the potential window, indicating standard capacitive behavior of the double layer capacitors. The Nyquist plots tend to be vertical lines (Figure 3b), indicating that both SCs exhibit good capacitive performance. Although the PVDF-HFP/Et_4NBF_4-AN electrolyte is much thicker than the separator, the ohmic resistance (R_s) of the SC with the PVDF-HFP organogel electrolyte is close to that of the liquid electrolyte. The good electrochemical performance of the PVDF-HFP organogel electrolyte is attributed to an ideally interconnected porous structure and good affinity toward acetonitrile resulting from the close solubility parameters of PVDF (23.2 $MPa^{1/2}$) and acetonitrile (24.2 $MPa^{1/2}$).[56,57]

With the lack of electroactive sites for pseudocapacitance, SCs based on pure CNT paper only deliver small specific capacitance. Therefore, the PDAA with high pseudocapacitance is introduced to CNT paper by the electrochemical polymerization method to improve capacitance. The chemical structures of CNT, PDAA, and CNT@PDAA are characterized by ATR-FTIR analysis. As shown in Figure 4a, no obvious absorption peak can be observed for pure CNT paper. After growing for 2.5 C cm^{-2}, the FTIR spectrum of CNT@PDAA is completely distinguished from the CNT film. The characteristic peaks of CNT@PDAA at 1575, 1491, and 1256 cm^{-1} are assigned to C═C stretching vibrations of quinoid and benzenoid rings as well as the C−N stretching vibration, similar to pure PDAA. This indicates that the PDAA successfully deposits onto the surface of CNT after electrochemical polymerization.

To determine the composition of the CNT@PDAA composite film, thermal gravimetric analysis (TGA) was performed (Figure 4b). It is clear from TGA curves that all the samples have a little mass loss around 100 °C due to the removing of adsorbed water. Pure CNT keeps about 94% weight, while pure PDAA exhibits about 71% weight residual at 800 °C. With the incorporation of CNT into PDAA, the CNT@PDAA composite shows about 78% weight residual at 800 °C, indicating improved thermal stability. On the basis of the weight residuals of CNT, PDAA, and CNT@PDAA at 800 °C, the PDAA content of the CNT@PDAA composite (2.5 C cm^{-2}) was calculated to be 69% (Supporting Information), which is very close to the result calculated by the weighing method (68%).

The morphologies of pure CNT paper and CNT@PDAA film were observed by FE-SEM. As shown in Figure 4c, pure CNT paper was composed of entangled carbon nanotubes with diameters of 10−30 nm. After electropolymerization for 2.5 C cm^{-2}, a shell/core coaxial heterostructure with tubular morphology was observed (Figure 4d). The diameter of the shell/core CNT@PDAA is about 50 nm. That is to say, the thickness of the PDAA shell is approximately in the range of 10−20 nm. A more detailed microstructure about the shell/core CNT@PDAA nanotubes is demonstrated by the high-magnification image shown in Figure S3. The surface of the CNT@PDAA nanotubes is rough and evenly covered with dense PDAA nanoparticles.

Figure 5a shows the cyclic voltammetry (CV) curve for CNT@PDAA measured by a three-electrode configuration in a 1 M Et_4NBF_4-AN electrolyte. The CV curve has two sets of redox responses, one appearing in a relatively negative potential range (from −1.8 to −1.0 V vs Ag/Ag^+) and the other in a more positive range (from 0 to +0.8 V). In the relatively negative potential range, two pairs of redox peaks at about −1.65 and −1.4 V correspond to the quinine/quinine radical anion ($Q/Q^{\bullet -}$) and quinine radical anion/quinine dianion ($Q^{\bullet -}/Q^{2-}$) transition, respectively (Figure 5b). The Et_4N^+ cations of the electrolyte compensate for the negative charges of $Q^{\bullet -}$ and Q^{2-} (n-doping). As the potential was taken more positive, the polyaniline moiety for PDAA is first oxidized to form a radical cation and further oxidized into an imine cation (=N^+−), which corresponds to a p-doping reaction with the BF_4^- anion insertion, bringing about the oxidation peaks of +0.35 and +0.59 V. Due to different redox reactions, a larger CV integral area of CNT@PDAA is obtained at a relatively negative potential range, while smaller at more positive

DOI: 10.1021/acssuschemeng.5b00334
ACS Sustainable Chem. Eng. 2015, 3, 2067−2076

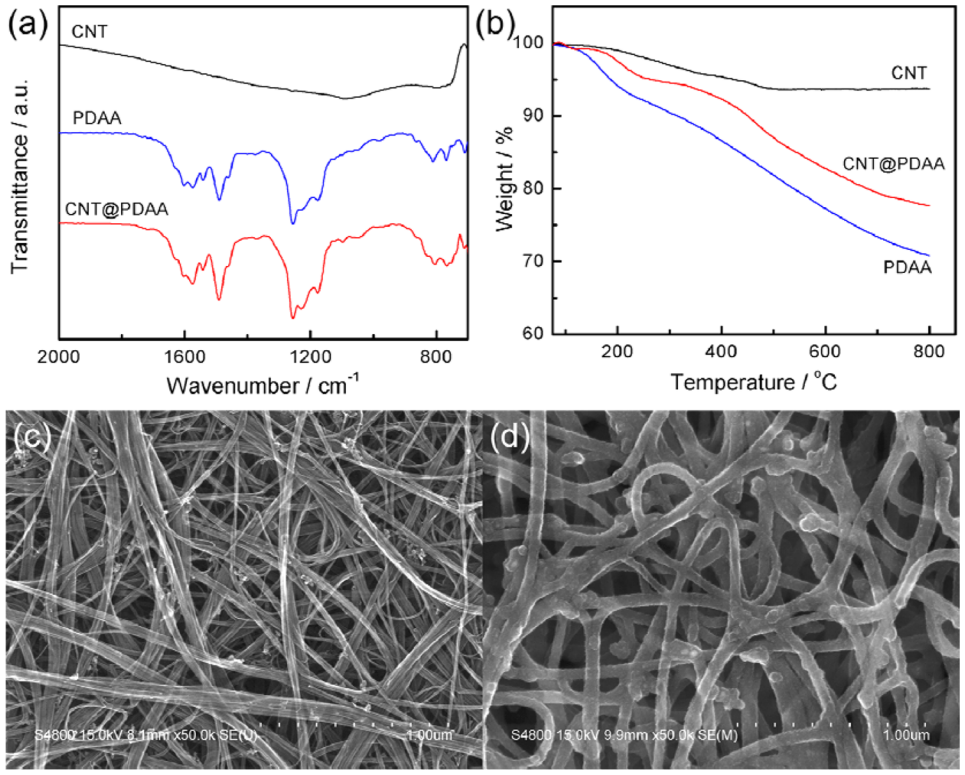

Figure 4. (a) FTIR spectra and (b) TG curves of CNT paper, PDAA, and CNT@PDAA film grown for 2.5 C cm^{-2}. FE-SEM images of (c) CNT paper and (d) CNT@PDAA film grown for 2.5 C cm^{-2}.

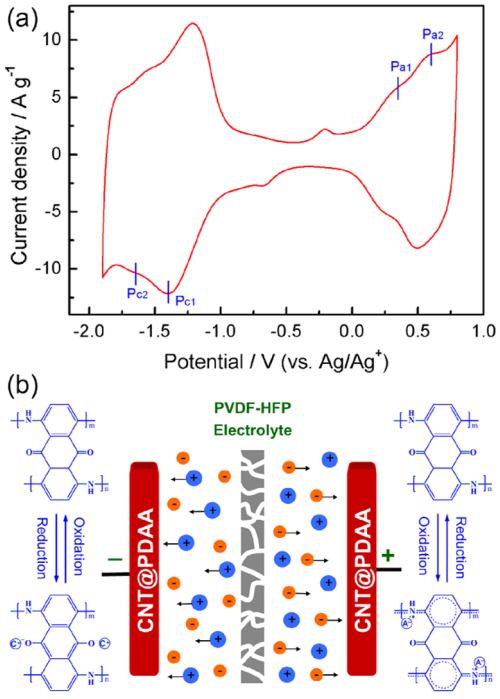

Figure 5. (a) CV curve of the CNT@PDAA (2.5 C cm^{-2}) film electrode at a scan rate of 20 mV s^{-1} in three-electrode mode. (b) Charge−discharge schematic illustration attaching corresponding redox reactions of CNT@PDAA film electrodes.

potential range, indicating that CNT@PDAA possesses higher specific capacitance as the negative electrode.

To estimate the optimal polymerization charge density of CNT@PDAA as the positive electrode (−0.55 to 0.8 V), the specific capacitances of CNT@PDAA with different charge densities at various current densities were systematically investigated (Figure S4). It is found that the specific capacitance gradually increases with an increase in polymerization charge density and reaches the highest value of 139 F g^{-1} at 2.5 C cm^{-2}. Subsequently, the specific capacitance and rate performance become worse, as the polymerization charge density continues to increase (3 C cm^{-2}). Thus, the CNT@PDAA composite film grown for 2.5 C cm^{-2} is optimum and chosen as the positive electrode for the flexible SC device.

In order to avoid excessive charge−discharge, it is crucial to balance the charges ($q^+ = q^-$) stored at the positive and negative electrodes for CNT@PDAA due to different redox reactions. The stored charges can be expressed according to the following equation:

$$q = C_s \times m \times U \tag{5}$$

where C_s is the specific capacitance, m is the mass of the electrode, and U is the potential window. To explore the appropriate polymerization charge density for CNT@PDAA as the negative electrode, a series of flexible SCs based on CNT@PDAA with different charge densities as the negative electrode were assembled. The appearance of the prototype CNT@PDAA//PVDF-HFP/Et_4NBF_4-AN//CNT@PDAA SC device is shown in Figure S5. As shown in Figure S6, the CV curves of SC-0.7 and SC-2.5 deviate seriously and show spindle shapes, which is ascribed to a severe charge imbalance between the positive and negative electrodes. In particular, the reduction peaks move to positive potential for SC-1.5. Furthermore, a comparison of specific capacitances at different current densities is reflected in Figure S7. Obviously, the highest specific capacitance at 5−30 mA cm^{-2} and excellent rate performance can be obtained using CNT@PDAA of 1.5 C

DOI: 10.1021/acssuschemeng.5b00334
ACS Sustainable Chem. Eng. 2015, 3, 2067−2076

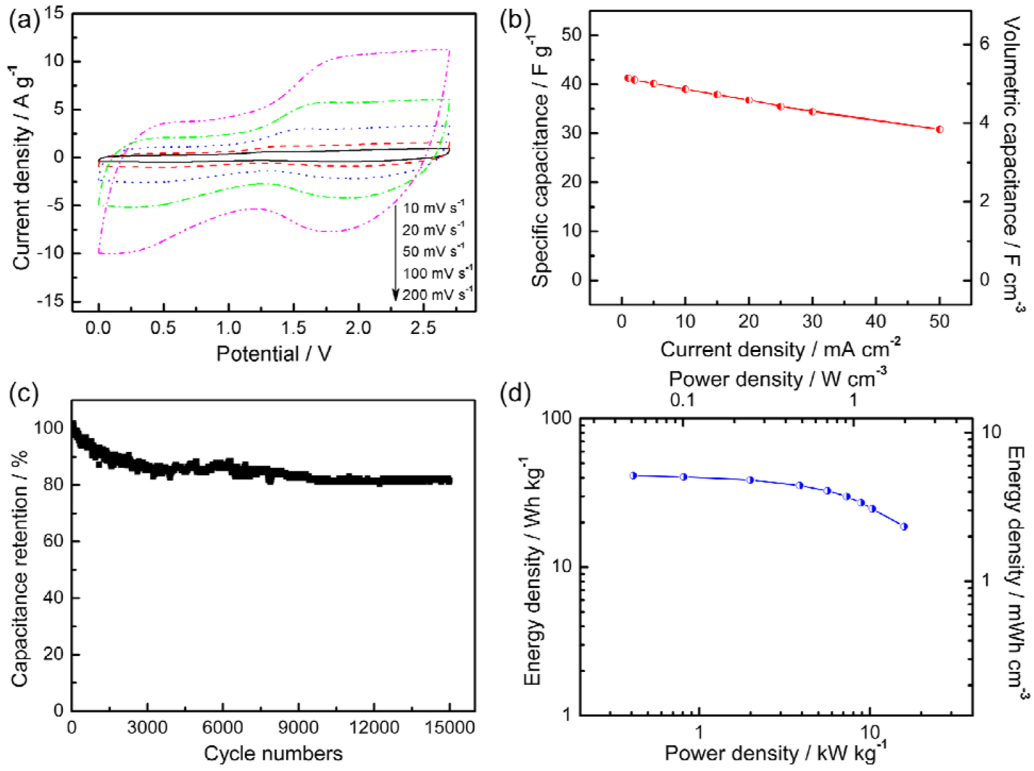

Figure 6. Electrochemical performance of the CNT@PDAA//PVDF-HFP/Et_4NBF_4-AN//CNT@PDAA supercapacitor (SC-1.5). (a) CV curves at different scan rates. (b) Specific capacitances and volumetric capacitances at various current densities. (c) Cycle performance at a current density of 2 mA cm^{-2}. (d) Ragone plot.

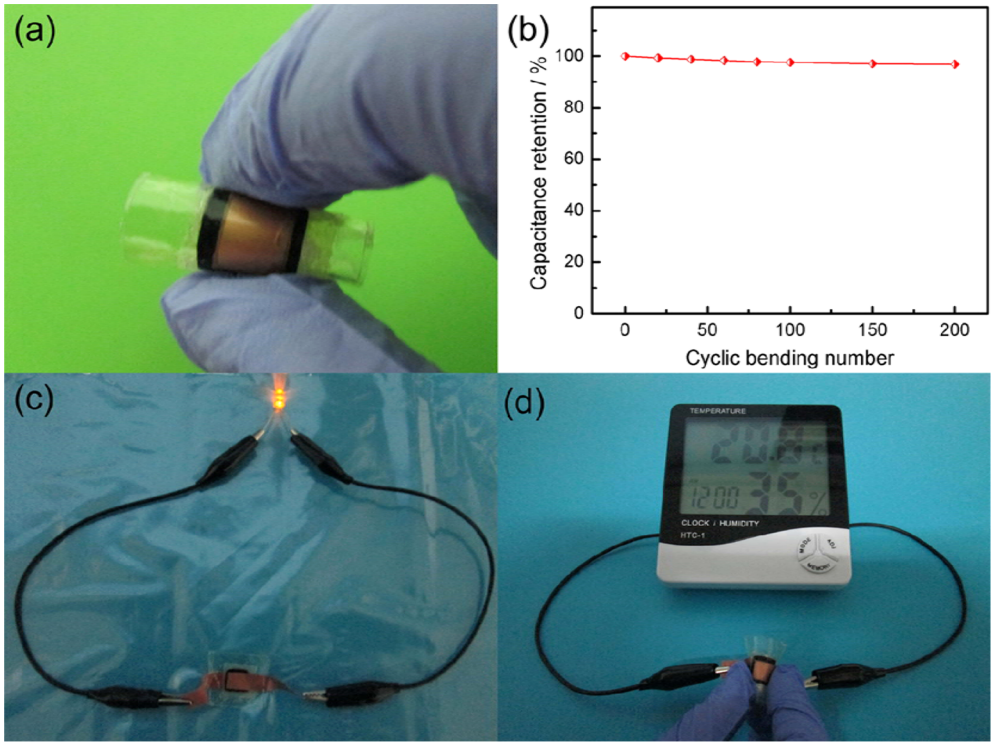

Figure 7. (a) Flexible supercapacitor (SC-1.5) under bending situation. (b) Capacitance retention after cyclic bending at angle of 145° for flexible supercapacitor (SC-1.5). (c) Photograph of a yellow LED lighted by a flexible supercapacitor (SC-1.5). (d) Photograph of a monitor powered by a flexible supercapacitor (SC-1.5) with bent state.

cm^{-2} as the negative electrode for flexible SCs. Thus, from the above, the optimal polymerization charge density for CNT@PDAA as the negative electrode is confirmed to be 1.5 C cm^{-2}.

In addition, the capacitive performance of the flexible SC-1.5 device was further evaluated, as shown in Figure 6. The perfect rectangular curves are not observed for the flexible SC device,

DOI: 10.1021/acssuschemeng.5b00334
ACS Sustainable Chem. Eng. 2015, 3, 2067−2076

indicating the pseudocapacitive characteristic of CNT@PDAA (Figure 6a). Meanwhile, the broad redox peaks are still robust enough at a high scan rate of 200 mV s^{-1}, which demonstrates the fast charge−discharge characteristics for the flexible SC. The charge curves of flexible SC-1.5 are almost symmetrical to the corresponding discharge parts, indicating that the redox reaction of CNT@PDAA is reversible (Figure S8). Calculating from the discharge curve based on the total mass of two electrodes, the specific capacitance of flexible SC-1.5 reaches up to 41.3 F g^{-1} at 1 mA cm^{-2} (Figure 6b). Flexible SC-1.5 retains 75% of the initial capacitance as the current density increases to 50 mA cm^{-2}. More importantly, the volumetric capacitance (including the volume of two electrodes and organogel electrolyte) of flexible SC-1.5 achieves 5.2 F cm^{-3} at 1 mA cm^{-2}, which is much higher than the value reported for other flexible SC devices.[58−61] Besides, flexible SC-1.5 exhibits low ohmic resistance (R_s) and charge-transfer resistance (R_{CT}) of 1.8 and 3.8 Ω, respectively (Figure S9).

To investigate the cycling stability of the flexible device, we subjected it to continuous charge−discharge tests for up to 15,000 cycles within 0−2.7 V at a current density of 2 mA cm^{-2}. As shown in Figure 6c, the main loss of specific capacitance occurs in the initial 2000 cycles (88% remained), and the capacitance retention still keeps 82% after 15,000 cycles, indicating relatively good reversibility and stability of the flexible device. To provide a comprehensive perspective on the capacitor performance, the Ragone plot of the flexible SC-1.5 device was provided. As shown in Figure 6d, the energy density of flexible SC-1.5 can reach up to 41.4 Wh kg^{-1} (5.16 mWh cm^{-3}) at a power density of 0.41 kW kg^{-1} (0.051 W cm^{-3}) and still remains 18.8 Wh kg^{-1} (2.34 mWh cm^{-3}) at a power density of 15.9 kW kg^{-1} (1.98 W cm^{-3}). This is superior or at least comparable to other reported flexible devices with organic electrolytes or ionic liquids, including carbon//PAN-*b*-PEG-*b*-PAN/$LiClO_4$-DMF//carbon (11.5 Wh kg^{-1}, 10 kW kg^{-1}),[21] RGO/V_2O_5//$LiClO_4$−PC//RGO (13.3 Wh kg^{-1}, 12.5 kW kg^{-1}),[62] and PEDOT//PVDF-HFP/$BMIBF_4$//PEDOT (6.5 Wh kg^{-1}, 11.3 kW kg^{-1}).[63] The high energy density can be attributed to the following factors. First, the ideally interconnected porous structure of the PVDF-HFP/Et_4NBF_4-AN electrolyte is favorable for rapid ion transport, which guarantees a rapid redox reaction for SCs. Second, unique p- and n-doping characteristics of PDAA contributes to a broad electroactive potential window and high specific capacitance of the electrodes. Third, the nanosized shell layer of PDAA greatly increases PDAA utilization and facilitates the migration of electrolyte ions during rapid redox reactions.

As shown in Figure 7a, as-prepared SC-1.5 exhibits an outstanding flexibility and can be bent arbitrarily without any harm to its structural integrity due to the combination of gel electrolyte, flexible free-standing electrodes, and packaging materials. More importantly, the durability performance under cyclic bending was addressed, which is evaluated by galvanostatic charge−discharge tests after repeated bending at an angle of ca. 145°. As shown in Figure 7b, the fading of specific capacitance is tiny and negligible, revealing good stability and capacitive performance of as-fabricated SC-1.5 under repeated bending. This further confirms the excellent flexibility of the as-prepared SC-1.5 device. In order to further evaluate the practical application of the flexible SC, one unit of the assembled device is used to power up commercial devices. A yellow LED has been successfully lightened by only one SC-1.5 device, as shown in Figure 7c. More importantly, the as-prepared SC-1.5 device can also drive a monitor in highly flexed state (Figure 7d). All these results demonstrate the application prospects for as-fabricated organic flexible SCs.

CONCLUSIONS

We have successfully developed a novel organic flexible SC device with a cross-linked PVDF-HFP porous organogel electrolyte sandwiched by two separated CNT@PDAA film electrodes. The highly porous PVDF-HFP membrane absorbs the liquid electrolyte 250% and displays high ionic conductivity of 14.4 × 10^{-3} S cm^{-1} at 25 °C. The PVDF-HFP organogel electrolyte demonstrates excellent nonflammability and a broad electrochemical stable window of 2.9 V. The as-assembled flexible SC exhibits a high volumetric capacitance of 5.2 F cm^{-3} at a current density of 1 mA cm^{-2} with a corresponding energy density of 41.4 Wh kg^{-1} (5.16 mWh cm^{-3}). Moreover, the flexible SC device also possesses excellent cycling stability of 82% capacitance retention rate after 15,000 charging−discharging cycles. More importantly, the flexible SC displays negligible degradation of electrochemical performance after repeated bending. The flexible device can drive commercially available products and hold great promise for application in portable and wearable electronics.

ASSOCIATED CONTENT

Supporting Information

XRD and DSC curves of porous PVDF-HFP membranes, FE-SEM image of CNT@PDAA, photograph and schematic diagram of the prototype flexible supercapacitor, electrochemical performance of flexible supercapacitors, and data analysis of electrochemical measurements and TGA. The Supporting Information is available free of charge on the ACS Publications website at DOI: 10.1021/acssuschemeng.5b00334.

AUTHOR INFORMATION

Corresponding Author

*Tel.: +86-21-64253527. E-mail: gengchaow@ecust.edu.cn.

Author Contributions

C. Yang and M. Sun contributed equally to this work.

Notes

The authors declare no competing financial interest.

ACKNOWLEDGMENTS

We greatly appreciate the financial supports of the National Natural Science Foundation of China (51173042) and Shanghai Municipal Science and Technology Commission (12 nm0504102).

REFERENCES

(1) Yang, P. H.; Mai, W. J. Flexible solid-state electrochemical supercapacitors. *Nano Energy* **2014**, *8*, 274−290.

(2) Peng, X.; Peng, L.; Wu, C. Z.; Xie, Y. Two dimensional nanomaterials for flexible supercapacitors. *Chem. Soc. Rev.* **2014**, *43*, 3303−3323.

(3) Lu, X. H.; Yu, M. H.; Wang, G. M.; Tong, Y. X.; Li, Y. Flexible solid-state supercapacitors: design, fabrication and applications. *Energy Environ. Sci.* **2014**, *7*, 2160−2181.

(4) Sumboja, A.; Foo, C. Y.; Wang, X.; Lee, P. S. Large areal mass, flexible and free-standing reduced graphene oxide/manganese dioxide paper for asymmetric supercapacitor device. *Adv. Mater.* **2013**, *25*, 2809−2815.

DOI: 10.1021/acssuschemeng.5b00334
ACS Sustainable Chem. Eng. 2015, 3, 2067−2076

(5) Lee, J. A.; Shin, M. K.; Kim, S. H.; Cho, H. U.; Spinks, G. M.; Wallace, G. G.; Lima, M. D.; Lepró, X.; Kozlov, M. E.; Baughman, R. H.; Kim, S. J. Ultrafast charge and discharge biscrolled yarn supercapacitors for textiles and microdevices. *Nat. Commun.* **2013**, *4*, 1970.
(6) Sellam; Hashmi, S. A. High rate performance of flexible pseudocapacitors fabricated using ionic-liquid-based proton conducting polymer electrolyte with poly(3,4-ethylenedioxythiophene):poly(styrene sulfonate) and its hydrous ruthenium oxide composite electrodes. *ACS Appl. Mater. Interfaces* **2013**, *5*, 3875−3883.
(7) Li, X.; Gu, T.; Wei, B. Dynamic and galvanic stability of stretchable supercapacitors. *Nano Lett.* **2012**, *12*, 6366−6371.
(8) Fei, H. J.; Yang, C. Y.; Bao, H.; Wang, G. C. Flexible all-solid-state supercapacitors based on graphene/carbon black nanoparticle film electrodes and cross-linked poly(vinyl alcohol)-H_2SO_4 porous gel electrolytes. *J. Power Sources* **2014**, *266*, 488−495.
(9) Li, L.; Zhang, X.; Qiu, J.; Weeks, B. L.; Wang, S. Reduced graphene oxide-linked stacked polymer forests for high energy-density supercapacitor. *Nano Energy* **2013**, *2*, 628−635.
(10) Lei, Z.; Liu, Z.; Wang, H.; Sun, X.; Lu, L.; Zhao, X. S. A high-energy-density supercapacitor with grapheme-CMK-5 as the electrode and ionic liquid as the electrolyte. *J. Mater. Chem. A* **2013**, *1*, 2313−2321.
(11) Zhang, F.; Lu, Y.; Yang, X.; Zhang, L.; Zhang, T.; Leng, K.; Wu, Y.; Huang, Y.; Ma, Y.; Chen, Y. A flexible and high-voltage internal tandem supercapacitor based on graphene-based porous materials with ultrahigh energy density. *Small* **2014**, *10* (11), 2285−2292.
(12) Zhao, J. W.; Chen, J. L.; Xu, S. M.; Shao, M. F.; Zhang, Q.; Wei, F.; Ma, J.; Wei, M.; Evans, D. G.; Duan, X. Hierarchical NiMn layered double hydroxide/carbon nanotubes architecture with superb energy density for flexible supercapacitors. *Adv. Funct. Mater.* **2014**, *24*, 2938−2946.
(13) He, Y. M.; Chen, W. J.; Zhou, J. Y.; Li, X. D.; Tang, P. Y.; Zhang, Z. X.; Fu, J. C.; Xie, E. Q. Constructed uninterrupted charge-transfer pathways in three-dimensional micro/nanointerconnected carbon-based electrodes for high energy-density ultralight flexible supercapacitors. *ACS Appl. Mater. Interfaces* **2014**, *6*, 210−218.
(14) Kang, Y. J.; Chun, S.; Lee, S.; Kim, B.; Kim, J. H.; Chung, H.; Lee, S.; Kim, W. All-solid-State flexible supercapacitors fabricated with bacterial nanocellulose papers, carbon nanotubes, and triblock-copolymer ion gels. *ACS Nano* **2012**, *6*, 6400−6406.
(15) Yang, C. Y.; Shen, J. L.; Wang, C. Y.; Fei, H. J.; Bao, H.; Wang, G. C. All-solid-state asymmetric supercapacitor based on reduced graphene oxide/carbon nanotube and carbon fiber paper/polypyrrole electrodes. *J. Mater. Chem. A* **2014**, *2*, 1458−1464.
(16) Zhang, J. T.; Jiang, J. W.; Li, H. L.; Zhao, X. S. A high-performance asymmetric supercapacitor fabricated with graphene-based electrodes. *Energy Environ. Sci.* **2011**, *4*, 4009−4015.
(17) Karthikeyan, K.; Amaresh, S.; Aravindan, V.; Lee, Y. S. Microwave assisted green synthesis of MgO-carbon nanotube composites as electrode material for high power and energy density supercapacitors. *J. Mater. Chem. A* **2013**, *1*, 4105−4111.
(18) Österholm, A. M.; Shen, D. E.; Dyer, A. L.; Reynolds, J. R. Optimization of PEDOT films in ionic liquid supercapacitors: demonstration as a power source for polymer electrochromic devices. *ACS Appl. Mater. Interfaces* **2013**, *5*, 13432−13440.
(19) Young, W. S.; Albert, J. N. L.; Schantz, A. B.; Epps, T. H. Mixed-salt effects on the ionic conductivity of lithium-doped PEO-containing block copolymers. *Macromolecules* **2011**, *44*, 8116−8123.
(20) Jung, H. R.; Lee, W. J. Electrochemical characteristics of electrospun poly(methyl methacrylate)/polyvinyl chloride as gel polymer electrolytes for lithium ion battery. *Electrochim. Acta* **2011**, *58*, 674−680.
(21) Huang, C.; Wu, C.; Hou, S.; Kuo, P.; Hsieh, C.; Teng, H. Gel electrolyte derived from poly(ethylene glycol) blending poly(acrylonitrile) applicable to roll-to-roll assembly of electric double layer capacitors. *Adv. Funct. Mater.* **2012**, *22*, 4677−4685.
(22) Rajendran, S.; Prabhu, M. R.; Rani, M. U. Ionic conduction in poly(vinyl chloride)/poly(ethyl methacrylate)-based polymer blend electrolytes complexed with different lithium salts. *J. Power Sources* **2008**, *180*, 880−883.
(23) Rodríguez, J.; Navarrete, E.; Dalchiele, E. A.; Sánchez, L.; Ramos-Barrado, J. R.; Martín, F. Polyvinylpyrrolidone-$LiClO_4$ solid polymer electrolyte and its application in transparent thin film supercapacitors. *J. Power Sources* **2013**, *237*, 270−276.
(24) Prasanth, R.; Shubha, N.; Hng, H. H.; Srinivasan, M. Effect of nano-clay on ionic conductivity and electrochemical properties of poly(vinylidene fluoride) based nanocomposite porous polymer membranes and their application as polymer electrolyte in lithium ion batteries. *Eur. Polym. J.* **2013**, *49*, 307−318.
(25) Zhu, Y. S.; Xiao, S. Y.; Shi, Y.; Yang, Y. Q.; Hou, Y. Y.; Wu, Y. P. A composite gel polymer electrolyte with high performance based on poly(vinylidene fluoride) and polyborate for lithium ion batteries. *Adv. Energy Mater.* **2014**, *4*, 1300647.
(26) Costa, C. M.; Silva, M. M.; Lanceros-Méndez, S. Battery separators based on vinylidene fluoride (VDF) polymers and copolymers for lithium ion battery applications. *RSC Adv.* **2013**, *3*, 11404−11417.
(27) Ahn, S. K.; Ban, T.; Sakthivel, P.; Lee, J. W.; Gal, Y.; Lee, J.; Kim, M.; Jin, S. Development of dye-Sensitized solar cells composed of liquid crystal embedded, electrospun poly(vinylidene fluoride-co-hexafluoropropylene) nanofibers as polymer gel electrolytes. *ACS Appl. Mater. Interfaces* **2012**, *4*, 2096−2100.
(28) Huang, F. L.; Xu, Y. F.; Peng, B.; Su, Y. F.; Jiang, F.; Hsieh, Y.; Wei, Q. F. Coaxial electrospun cellulose-core fluoropolymer-shell fibrous membrane from recycled cigarette filter as separator for high performance lithium-ion battery. *ACS Sustainable Chem. Eng.* **2015**, *3*, 932−940.
(29) Cheng, Q.; Cui, Z. Y.; Li, J. B.; Qin, S. H.; Yan, F.; Li, J. X. Preparation and performance of polymer electrolyte based on poly(vinylidene fluoride)/polysulfone blend membrane via thermally induced phase separation process for lithium ion battery. *J. Power Sources* **2014**, *266*, 401−413.
(30) Yang, X.; Zhang, F.; Zhang, L.; Zhang, T. F.; Huang, Y.; Chen, Y. S. A high-performance graphene oxide-doped ion gel as gel polymer electrolyte for all-solid-state supercapacitor applications. *Adv. Funct. Mater.* **2013**, *23*, 3353−3360.
(31) Costa, C. M.; Rodrigues, L. C.; Sencadas, V.; Silva, M. M.; Rocha, J. G.; Lanceros-Méndez, S. Effect of degree of porosity on the properties of poly(vinylidene fluoride-trifluorethylene) for Li-ion battery separators. *J. Membr. Sci.* **2012**, *407−408*, 193−201.
(32) Jeschke, S.; Mutke, M.; Jiang, Z. X.; Alt, B.; Wiemhöfer, H. D. Study of carbamate-modified disiloxane in porous PVDF-HFP membranes: new electrolytes/separators for lithium-ion batteries. *ChemPhysChem* **2014**, *15*, 1761−1771.
(33) Shalu; Chaurasia, S. K.; Singh, R. K.; Chandra, S. Thermal stability, complexing behavior, and ionic transport of polymeric gel membranes based on polymer PVdF-HFP and ionic liquid, [BMIM]-[BF_4]. *J. Phys. Chem. B* **2013**, *117*, 897−906.
(34) Xiong, M.; Tang, H. L.; Wang, Y. D.; Lin, Y.; Sun, M. L.; Yin, Z. F.; Pan, M. Expanded polytetrafluoroethylene reinforced polyvinylidenefluoride-hexafluoropropylene separator with high thermal stability for lithium-ion batteries. *J. Power Sources* **2013**, *241*, 203−211.
(35) Zhang, J. Q.; Chen, S. Q.; Xie, X. Q.; Kretschmer, K.; Huang, X. D.; Sun, B.; Wang, G. X. Porous poly(vinylidene fluoride-co-hexafluoropropylene) polymer membrane with sandwich-like architecture for highly safe lithium ion batteries. *J. Membr. Sci.* **2014**, *472*, 133−140.
(36) Dumas, L.; Fleury, E.; Portinha, D. Wettability adjustment of PVDF surfaces by combining radiation-induced grafting of (2,3,4,5,6)-pentafluorostyrene and subsequent chemoselective "click-type" reaction. *Polymer* **2014**, *55*, 2628−2634.
(37) Salinas-Torres, D.; Shiraishi, S.; Morallón, E.; Cazorla-Amorós, D. Improvement of carbon materials performance by nitrogen functional groups in electrochemical capacitors in organic electrolyte at severe conditions. *Carbon* **2015**, *82*, 205−213.
(38) Li, Y. Y.; Li, Z. S.; Shen, P. K. Simultaneous formation of ultrahigh surface area and three-dimensional hierarchical porous

DOI: 10.1021/acssuschemeng.5b00334
ACS Sustainable Chem. Eng. 2015, 3, 2067−2076

graphene-like networks for fast and highly stable supercapacitors. *Adv. Mater.* **2013**, *25*, 2474−2480.
(39) Cho, W.; Yeom, C. G.; Kim, B. C.; Kim, K. M.; Ko, J. M.; Yu, K. Supercapacitive properties of activated carbon electrode in organic electrolytes containing single- and double-cationic liquid salts. *Electrochim. Acta* **2013**, *89*, 807−813.
(40) Zhou, S. P.; Zhang, H. M.; Zhao, Q.; Wang, X. H.; Li, J.; Wang, F. S. Graphene-wrapped polyaniline nanofibers as electrode materials for organic supercapacitors. *Carbon* **2013**, *52*, 440−450.
(41) Kim, M.; Lee, C.; Jang, J. Fabrication of highly flexible, scalable, and high-performance supercapacitors using polyaniline/reduced graphene oxide film with enhanced electrical conductivity and crystallinity. *Adv. Funct. Mater.* **2014**, *24*, 2489−2499.
(42) Wang, Z. H.; Tammela, P.; Strømme, M.; Nyholm, L. Nanocellulose coupled flexible polypyrrole@graphene oxide composite paper electrodes with high volumetric capacitance. *Nanoscale* **2015**, *7*, 3418−3423.
(43) Ni, T.; Xu, L.; Sun, Y. P.; Yao, W.; Dai, T. Y.; Lu, Y. Facile fabrication of reduced graphene oxide/polypyrrole composite hydrogels with excellent electrochemical performance and compression capacity. *ACS Sustainable Chem. Eng.* **2015**, *3*, 862−870.
(44) Sun, M. Q.; Wang, G. C.; Yang, C. Y.; Jiang, H.; Li, C. Z. A graphene/carbon nanotube@π-conjugated polymer nanocomposite for high-performance organic supercapacitor electrodes. *J. Mater. Chem. A* **2015**, *3*, 3880−3890.
(45) Sun, M. Q.; Tang, Q. Q.; Zhang, T.; Wang, G. C. Rational synthesis of novel π-conjugated poly(1,5-diaminoanthraquinone) for high-performance supercapacitors. *RSC Adv.* **2014**, *4*, 7774−7779.
(46) Liu, H. Y.; Zhang, G. Q.; Zhou, Y. F.; Gao, M. M.; Yang, F. L. One-step potentiodynamic synthesis of poly(1,5-diaminoanthraquinone)/reduced graphene oxide nanohybrid with improved electrocatalytic activity. *J. Mater. Chem. A* **2013**, *1*, 13902−13913.
(47) Li, X. G.; Li, H.; Huang, M. R. Productive synthesis and properties of polydiaminoanthraquinone and its pure self-stabilized nanoparticles with widely adjustable electroconductivity. *Chem. - Eur. J.* **2007**, *13*, 8884−8896.
(48) Noël, V.; Randriamahazaka, H. N. Redox-assisted hydrogen bonding within interpenetrating conducting polymer networks for charge-storage materials. *Electrochem. Commun.* **2012**, *19*, 32−35.
(49) Hashmi, S. A.; Suematsu, S.; Naoi, K. All solid-state redox supercapacitors based on supramolecular 1,5-diaminoanthraquinone oligomeric electrode and polymeric electrolytes. *J. Power Sources* **2004**, *137*, 145−151.
(50) Naoi, K.; Suematsu, S.; Hanada, M.; Takenouchi, H. Enhanced cyclability of π-π stacked supramolecular 1,5-diaminoanthraquinone oligomer as an electrochemical capacitor material. *J. Electrochem. Soc.* **2002**, *149*, A472−A477.
(51) Deng, B.; Yu, M.; Yang, X. X.; Zhang, B. W.; Li, L. F.; Xie, L. D.; Li, J. Y.; Lu, X. F. Antifouling microfiltration membranes prepared from acrylic acid or methacrylic acid grafted poly(vinylidene fluoride) powder synthesized via pre-irradiation induced graft polymerization. *J. Membr. Sci.* **2010**, *350*, 252−258.
(52) Karabelli, D.; Leprêtre, J. C.; Alloin, F.; Sanchez, J. Y. Poly(vinylidene fluoride)-based macroporous separators for supercapacitors. *Electrochim. Acta* **2011**, *57*, 98−103.
(53) Xiao, W.; Miao, C.; Yin, X.; Zheng, Y.; Tian, M.; Li, H.; Mei, P. Effect of urea as pore-forming agent on properties of poly(vinylidene fluoride-co-hexafluoropropylene)-based gel polymer electrolyte. *J. Power Sources* **2014**, *252*, 14−20.
(54) Xiao, W.; Li, X.; Guo, H.; Wang, Z.; Zhang, Y.; Zhang, X. Preparation of core-shell structural single ionic conductor SiO_2@Li^+ and its application in PVDF−HFP-based composite polymer electrolyte. *Electrochim. Acta* **2012**, *85*, 612−621.
(55) Ruch, P. W.; Cericola, D.; Foelske-Schmitz, A.; Kötz, R.; Wokaun, A. Aging of electrochemical double layer capacitors with acetonitrile-based electrolyte at elevated voltages. *Electrochim. Acta* **2010**, *55*, 4412−4420.
(56) Wang, K. Y.; Foo, S. W.; Chung, T.-S. Mixed matrix PVDF hollow fiber membranes with nanoscale pores for desalination through direct contact membrane distillation. *Ind. Eng. Chem. Res.* **2009**, *48*, 4474−4483.
(57) Cheng, Q. H.; Debnath, S.; O'Neill, L.; Hedderman, T. G.; Gregan, E.; Byrne, H. J. Systematic study of the dispersion of SWNTs in organic solvents. *J. Phys. Chem. C* **2010**, *114*, 4857−4863.
(58) El-Kady, M. F.; Strong, V.; Dubin, S.; Kaner, R. B. Laser scribing of high-performance and flexible graphene-based electrochemical capacitors. *Science* **2012**, *335*, 1326−1330.
(59) Xiao, J. W.; Xi, J. B.; Xu, Y. Y.; Yang, S. H.; Jin, Y. X.; Xiao, F.; Wang, S. Strongly coupled metal oxide nanorod arrays with grapheme nanoribbons and nanosheets enable novel solid-state hybrid cells. *J. Power Sources* **2015**, *283*, 95−103.
(60) Xiao, X.; Li, T.; Peng, Z.; Jin, H.; Zhong, Q.; Hu, Q.; Yao, B.; Luo, Q.; Zhang, C.; Gong, L.; Chen, J.; Gogotsi, Y.; Zhou, J. Freestanding functionalized carbon nanotube-based electrode for solid-state asymmetric supercapacitors. *Nano Energy* **2014**, *6*, 1−9.
(61) Yang, P.; Xiao, X.; Li, Y.; Ding, Y.; Qiang, P.; Tan, X.; Mai, W.; Lin, Z.; Wu, W.; Li, T.; Jin, H.; Liu, P.; Zhou, J.; Wong, C. P.; Wang, Z. L. Hydrogenated ZnO core-shell nanocables for flexible supercapacitors and self-powered systems. *ACS Nano* **2013**, *7*, 2617−2626.
(62) Foo, C. Y.; Sumboja, A.; Tan, D. J. H.; Wang, J. X.; Lee, P. S. Flexible and highly scalable V_2O_5-rGO electrodes in an organic electrolyte for supercapacitor devices. *Adv. Energy Mater.* **2014**, *4*, 1400236.
(63) Pandey, G. P.; Rastogi, A. C.; Westgate, C. R. All-solid-state supercapacitors with poly(3,4-ethylenedioxythiophene)-coated carbon fiber paper electrodes and ionic liquid gel polymer electrolyte. *J. Power Sources* **2014**, *245*, 857−865.

DOI: 10.1021/acssuschemeng.5b00334
ACS Sustainable Chem. Eng. 2015, 3, 2067−2076